

Citation for published version:

Balazs Ihracska, et al, 'Opto-mechanical design for sight windows under high loads', *Materials & Design*, Vol. 117: 430-444, March 2017.

DOI:

<https://doi.org/10.1016/j.matdes.2016.12.080>

Document Version:

This is the Accepted Manuscript version.

The version in the University of Hertfordshire Research Archive may differ from the final published version.

Copyright and Reuse:

© 2016 Elsevier Ltd.

This manuscript version is made available under the terms of the Creative Commons Attribution-NonCommercial-NoDerivatives License CC BY NC-ND 4.0

(<http://creativecommons.org/licenses/by-nc-nd/4.0/>), which permits non-commercial re-use, distribution, and reproduction in any medium, provided the original work is properly cited, and is not altered, transformed, or built upon in any way.

Enquiries

If you believe this document infringes copyright, please contact the Research & Scholarly Communications Team at rsc@herts.ac.uk

1 **Title: Opto-mechanical design for sight windows under high loads**

2 Journal: Materials & Design; <http://www.journals.elsevier.com/materials-and-design/>

3 Article type: Technical report

4

1*	Balazs Ihracska	University of Hertfordshire, School of Engineering and Technology, College Lane Hatfield, Hertfordshire AL10 9AB, UK	a.b.ihracska@herts.ac.uk
2	Roy James Crookes	School of Engineering and Materials Science, Queen Mary University of London, London E1 4NS, UK	r.j.crookes@qmul.ac.uk
3	Diogo Montalvão	Department of Design and Engineering, Faculty of Science and Technology, Bournemouth University, Talbot Campus, Fern Barrow, Poole, Dorset BH12 5BB, UK	dmontalvao@bournemouth.ac.uk
4	Mohammad Reza Herfatmanesh	University of Hertfordshire, School of Engineering and Technology, College Lane Hatfield, Hertfordshire AL10 9AB, UK	m.r.herfatmanesh@herts.ac.uk
5	Zhijun Peng	University of Hertfordshire, School of Engineering and Technology, College Lane Hatfield, Hertfordshire AL10 9AB, UK	z.peng2@herts.ac.uk
6	Shahid Imran	Department of Mechanical Engineering (KSK Campus), University of Engineering and Technology, Lahore, Pakistan	shahidimran512@hotmail.com
7	Theodosios Korakianitis	Parks College of Engineering, Aviation and Technology, Saint Louis University, St. Louis, MO 63103, USA	talexander@slu.edu

5 *corresponding author

6

7 **Abstract**

8

9 In this study, the design aspects of optically accessible pressure vessels are investigated via a case study of a High Pressure
10 Combustor experimental rig. The rig was designed to take optical measurements of combustion, simulating the conditions
11 found in internal combustion engines and turbines. Although, it is not new to equip chambers and reactors with sight
12 windows, important aspects of design and relevant information regarding optical access is missing or are insufficiently
13 explored or not readily accessible in the existing literature. A comprehensive review of requirements for optical access to
14 such high-pressure, high-temperature systems has been conducted. It is shown in a readily-navigable format as function of
15 application and precision, with data and technical correlations hitherto not found in a 'user-friendly' style. The material
16 selection procedure is detailed and supported by a complete comparison of optical materials and relevant properties. The
17 review revealed a significant inconsistency in mechanical properties claimed in the literature for optical materials. As a
18 response to this, increased safety factor values are suggested as function of level of uncertainties and effects of failure,
19 typically three to four times higher than the industrial standard. Moreover, newly developed equations are presented linking
20 performance analysis to the design criteria.

21

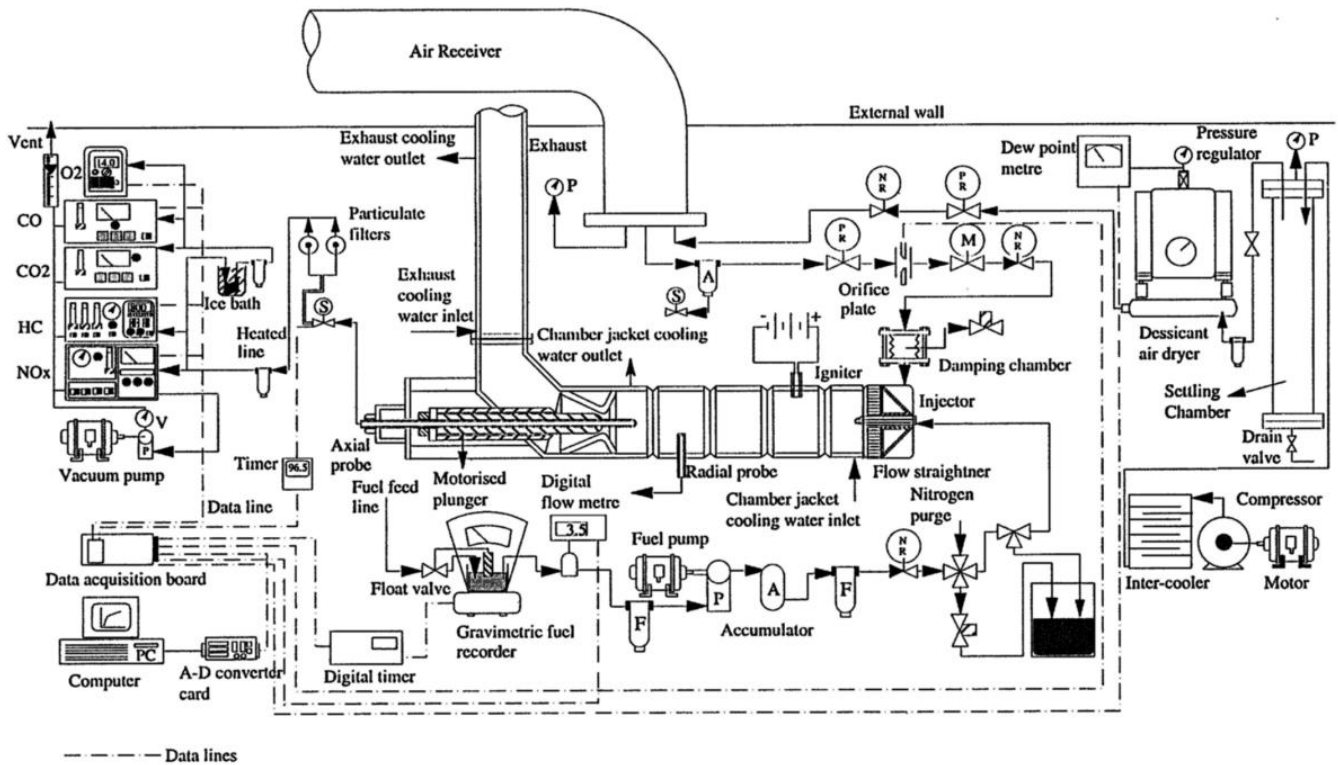
22 Keywords:

- 23 • Optically-accessible reactor,
- 24 • Optical engine,
- 25 • Pressure vessel;
- 26 • Sapphire,
- 27 • Window design,
- 28 • Combustion

29 1 Introduction to the High Pressure Combustor (HPC) and the need for optical development

30 Over the past two decades, concerns about global warming and the depletion of the ozone layer have driven researchers to
31 find better alternatives to the high energy consumption demand [1-4]. With the combustion of fossil fuel and the subsequent
32 production of carbon dioxide being accounted for as the main contributor to the current release of greenhouse gases to the
33 atmosphere [5], and taking into consideration that a solution to the current energy supply problems is yet distant,
34 improvements in the understanding of the chemical reaction and flame-propagation processes and reduction the emissions
35 of these engine-fuel combinations should be implemented as a short term solution [6-8].

36 The HPC was developed to address research topics in combustion science. Its unique design makes it a versatile tool to
37 model and test the working, at real-life conditions of industrial furnaces, external and internal combustion engines and gas
38 turbines. It can be set up to test steady combustion up to 60 bar for 30 minutes. It can accept virtually any combustible
39 substance with a high accuracy of air-fuel ratio and a control of residence time. Moreover, the flow pattern can be set to
40 either plug or swirl. The high-pressure air (variable up to 60 bar) is delivered to the chamber via a number of safety
41 instruments from a large air receiver – which is charged by a three-stage piston pump. The air arriving to the combustion
42 chamber is dried, and its flow and pressure is set by a computer-controlled valve system. The fuel is injected into the
43 chamber by interchangeable injectors; the fuel flow pattern, supply pressure and volume flow is variable. The actual
44 combustion chamber is not a single-piece vessel but rather an assembly of several sections. Therefore, the length of the
45 chamber – and hence, the residence time of reactants – can be varied depending on the application. The sections were
46 designed with numerous radial access points so that reaching any point inside the combustor for sampling would be
47 possible; see Figure 1 for a schematic of the experimental rig. The initial ignition is provided by a high-energy spark. At the
48 end of the process, the burned mixture leaves the chamber via a special plunger valve that is capable of withstanding the
49 high temperature and pressure. A detailed description of the HPC facility can be found in [9-11].



50

51

Figure 1. Schematic drawing of the experimental rig, adapted from [10].

52 The HPC has supplied the combustion research community with vital information. Using thermocouples and sample probes,
53 its current capabilities have been fully utilised. New developments were needed to keep the rig up-to-date. In the last 15
54 years or so, the optical- and laser-based measurements became the most important tools to investigate combustion details
55 and results of these methods published elsewhere [12-14]. These methods have a fast response time and do not require
56 actual physical contact with the flames. It was essential to equip the HPC with optical access in order to keep the research
57 work current and on-going.

58 2 Current contribution

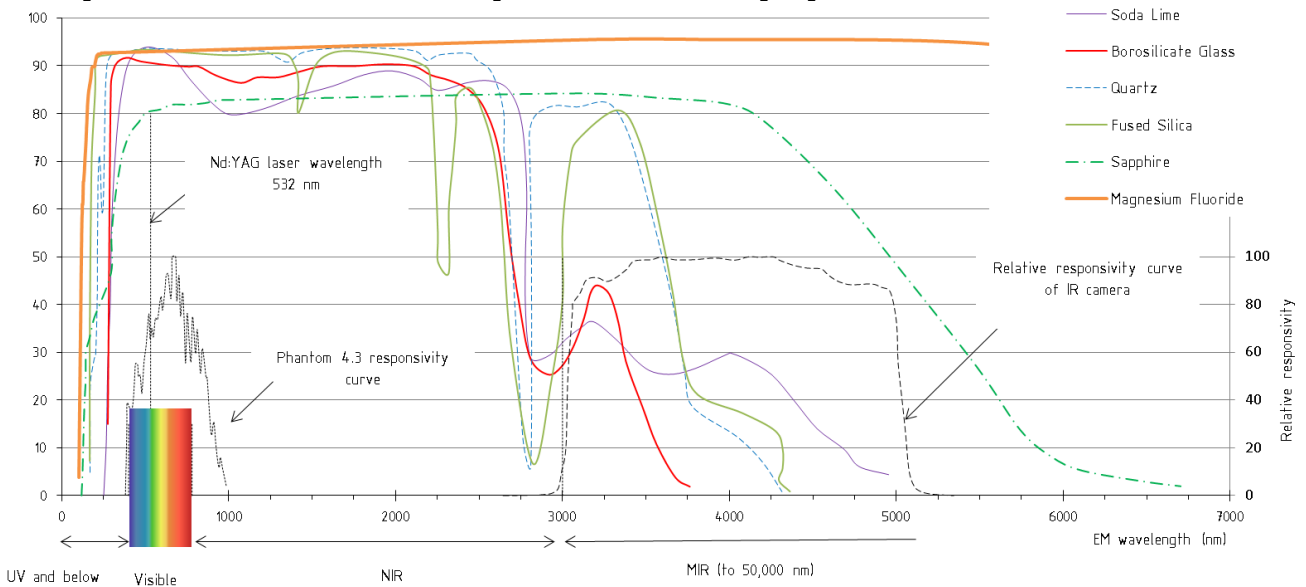
59 The design methods and procedures of industrial pressure vessels are well-documented, with comparisons of methods and
60 standards available for industrial applications [15-25]. These provide good guidelines even for an unconventional design
61 task, but of course they do not provide comprehensive data for all possible cases. In general, the available literature lacks

62 data regarding optical access to pressurised vessels. Information on design practices and material properties are scattered
63 in the literature, being hard to find and often inconsistent. Therefore, the aim of this work is to target these gaps by:
64 collecting the scattered data; dealing with inconsistency found in literature and providing detailed recommendation for
65 safety factors, collecting and presenting design criteria as function of application; developing new functions and equations.

66 In this work, novel complementary material is provided for the design of chambers and reactors that require the equipment
67 of sight windows on them. As a result of extensive review, the properties of practical optical materials were collected and
68 presented together in graphs and tables, allowing for direct comparison. The details of special design practices regarding
69 transparent parts are discussed, and the available data on existing design solutions is collected and shown. Some
70 complementary material is added to the basic equations and relations in Statics. Moreover, there are papers examining
71 design procedures [26], but to the authors' knowledge this is the first detailed design study on optically accessible pressure
72 vessels (fixed volume or internal combustion optical engine) where the real-life application of the collected data is shown.
73 Structural analysis of optical material window is shown and its effects to practical design.

74 3 The optical access: review of material and their properties; practical solutions; 75 mechanical and optical performance

76 3.1 Optical materials: mechanical, optical and chemical properties



77
78 **Figure 2 Transmittance of the reviewed optical materials; relative responsivity and wavelength of interest are also**
79 **shown (for Design requirements section).**

80 There are a large number of materials that can be considered for sight windows on pressure vessels, from ordinary plastics
81 to exotic ceramics. In this work, only the most common and most practical optical materials were chosen for comparison.

82 The underlying design criteria for selecting the optimal optical material type are: useful transmittance range, operating
83 temperature and mechanical load. In Table 1, only high-operating-temperature materials are listed. It is important to note
84 there are other choices available for specialised tasks, such as silicon or germanium, but their availability is limited and they
85 are costlier. In low-temperature environments, plastics like acrylic and polycarbonate can be used. During design, it is
86 essential to consider the working temperature and obtain a good estimate of it from simulations or experiments.

87 Although unusual in mechanical engineering, it is important to choose the right material for the required electromagnetic
88 band. It is also vital to consider the ratio of the electromagnetic energy falling on a body to that transmitted through it. This
89 ratio is called the transmittance of the material [27]. Transmittance values for each wavelength vary significantly among
90 material. For example, a larger selection of materials can be considered if the investigated radiation is in the visible or in the
91 near infra-red (NIR) regions. Due to the availability of a wider range of materials, the implication is that sight windows for
92 high speed imaging or laser-aided measurements can be designed more easily, and more complex shapes with larger
93 dimensions are therefore possible. Choosing an optimal material is more complex when longer wavelengths have to be
94 captured for both spectroscopy and thermal imaging. For wavelengths over 2500 nm, the transmittance curves start
95 fluctuating or becoming discontinuous. If this, then, is the electromagnetic wave band region of interest, careful planning
96 will be needed to select the right material type. The transmittance of common optical materials for wavelengths under 200-
97 250 nm falls rapidly. Yet, it is an important region in combustion science as some radicals have their peak emissivity in this

98 electromagnetic band. Researchers and designers are practically left with fused silica and a number of fluorides (MgF₂, CaF₂,
99 BaF₂) to use. Figure 2 shows the transmittance curves of selected materials.

100 Once the material candidates are shortlisted by wavelength transmittance, the more conventional design process follows
101 this when further mechanical, thermal and chemical resistance properties are of interest.

102 Finally, the cost analysis needs to be taken into account when the material type providing the optimal solution is chosen.

103 Table 1 summarises some of the most related properties of a selection of practical optical materials. As expected, all of the
104 listed properties are functions of temperature, size and shape, exact composition, heat treatment, surface finish, and other
105 manufacturing processes. It is important to note that there are significant differences (10-15%) between the claimed values
106 by different manufacturers and textbooks.

107

Table 1. Optical material properties

	Unit	Soda Lime Glass	Borosilicate	Quartz	Fused Silica	Sapphire	Magnesium Fluoride
General							
Chemical Formula, Composition	(weight %)	SiO ₂ :74, Na ₂ O:15, CaO:5, others	SiO ₂ :80+, B ₂ O ₃ :7-13, Na ₂ O, others	SiO ₂ :99	SiO ₂ :99	Al ₂ O ₃ :99	MgF ₂ :99
Density	(g/cm ³)	2.2-2.52	2.2-2.4	2.2	2.2	3.98	3.18
Optical							
Useful Transmission	(nm)	320-2300	325-2100	200-2400	180-2200	150-5000	110-7500
Refractive index (588 nm)	-	1.52	1.47	1.46	1.46	1.76	1.38
Mechanical^I							
Young's Modulus	(GPa)	72	64	73	73	335	138
Tensile Strength	(MPa)	41	27-62	50	50	275 ^{II}	140
Hardness, Vickers	-	550	520-580	1000-1200	1000-1200	1940	400
Poisson's ratio	-	0.23	0.21	0.17	0.17	0.25	0.27
Weibull variability of strength	-	6 ^{III}	30 ^{IV}	8.82 ^V	10.2 ^{VI}	5	5
Weibull stress	(MPa)	129 ^{III}	71 ^{IV}	115 ^V	180 ^{VI}	485	96
Thermal							
Softening Point	(°C)	1450	800-850	1730	1600	2300 ^{VII}	1255
Max. Continuous Operating Temperature	(°C)	260	280-350	950-1150	950-1100	1200	500
Thermal Conductivity at 300 K	(W/mK)	0.96	1.1-1.2	1.38	1.38	27.21	11.6
Coefficient of Expansion	(10 ⁻⁶ /K)	3.5-9	3.25-4	0.55	0.55	8.4	8.9

properties perpendicular to optical axis

materials are birefringent for exact refractive indexes see references

mechanical properties at room temperature

^I mechanical and optical properties are dependent on fabrication method and surface finish; ^{II} fractural strength; ^{III} Kimble R-6; ^{IV} BK-7; ^V standard polish; ^{VI} "super polish"; ^{VII} melting point

108

109 Soda lime glass is the common glass type that can be found everywhere. It is mass-manufactured by floating the hot raw
110 material on a bed of molten tin. It is the least expensive material of all, and being softer than other glasses, it is easy to make
111 a complex part out of it. It is a hard material with good scratch resistance, but is significantly softer than other glasses or
112 sapphire. It is not resistant to many chemicals, and its higher coefficient of expansion makes it sensitive to uneven
113 temperature distribution [28-32].

114 Borosilicate glass is 2-3 times more expensive than soda lime glass but still considerably less expensive than fused quartz or
115 silica. It has the same easy manufacturing properties as soda lime but usually has a lower thermal expansion coefficient,
116 hence making it more resistant to thermal shock. Leaching can occur but it is more resistant to chemicals [28-31, 33, 34].

117 Fused quartz and silica have very similar properties as they have an almost identical composition. The main difference
118 between them is in the amount of contamination caused by the different manufacturing processes. Quartz is made from
119 melted and cleansed naturally occurring quartz sand with larger amount of contamination in the product, while fused silica
120 is a pure version of quartz synthesised from various gases. However, their mechanical and electrical properties are identical.
121 The only contrasting (and significant) advantage is that, silica has an excellent transmittance in the ultra violet (UV) region.
122 This property makes it unique among silicon oxides. A major advantage of quartz and silica, when compared to cheaper
123 glasses, is their increased stability. Their mechanical properties are significantly less sensitive to temperature changes than
124 borosilicate or float glasses. For instance, for a borosilicate, the linear thermal expansion at 500 °C increases its ambient
125 value a few hundred times; silica, however, faces an increase of about 40 times and then stays constant with further increase
126 of the temperature. This makes the evaluation of thermal stresses a lot easier when implementing quartz and silica.
127 Nevertheless, their excellent properties come at a price: the material cost is significantly higher than the aforementioned
128 glasses and their higher temperature resistance makes fabrication more complex. They have a reasonably good resistance
129 to chemicals but break down with some caustics, fluorinated acids and plasmas [28-31, 33-36].

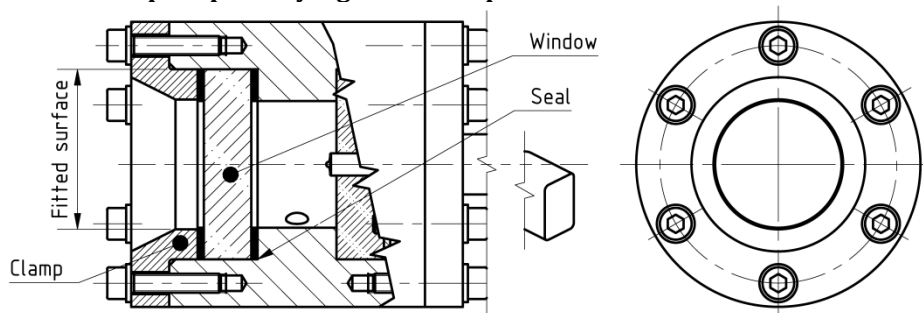
130 Sapphire is a single crystal and a very versatile material. It is the second hardest material on Earth, which makes it best
131 choice of material whenever wear and abrasion are the main constraints. Its high mechanical strength and modulus of
132 elasticity provides good resistance against impacts. It is virtually impervious to all corrosive materials and its thermal stability
133 outperforms all other optical materials. Yet, sapphire raw material is not significantly more expensive than fused silica. On
134 the other hand, its extreme hardness and a high melting point make the manufacturing process challenging and costly. In
135 conclusion, sapphire is not suitable for large windows and for complex shapes [37-43].

136 Magnesium fluoride is an excellent material choice for application in the UV bandwidth (the cheaper CaF₂ has similar
137 properties but with slightly reduced useful transmittance range). Larger size crystals can be grown, and it is possible to
138 machine it with standard diamond tools as this material can be polished well. Thus, complex shapes and geometries can be
139 achieved. It has a wide range of transmissivity but it is not as wear-resistant as the other materials, and its surface will
140 degrade in a humid environment at elevated temperatures (over 500 °C) [33, 39, 44-46].

141 3.2 Geometric design and mounting methods

142 There are a number of different ways to hold the optical element within an optical apparatus. A particular mounting method
143 can be selected considering the geometric constraints, the sealing requirements, position accuracy, the orientation of optical
144 axis, stress and the deformation caused by pressure difference, and birefringence. In this paper, sight optics is investigated
145 only; their mounts are less complex than lenses that need more degrees of freedom.

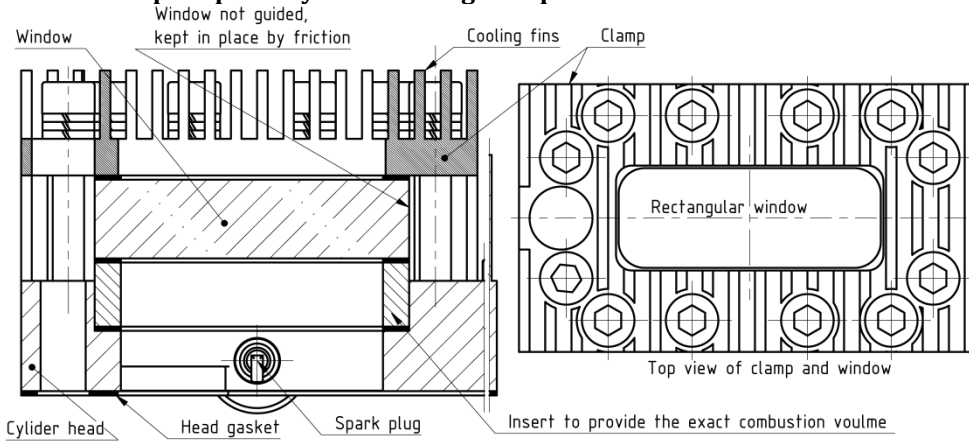
146 3.2.1 Optical element kept in place by a guided clamp



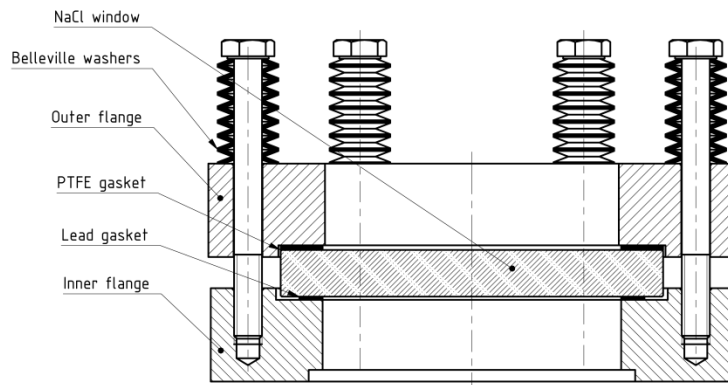
147
148 **Figure 3. Fixed volume combustion chamber with circular window that is positioned by a guided clamp [47].**

149 Figure 3 shows the usual clamping method where the retainer is fitted and guided in the direction of the displacement of
150 the window. The radial position of the retainer is fully defined by the contact forces. The advantage of this solution is the
151 simple tensile load on fixing bolts, and simplified dismantling and re-assembly. Details of loaded bolted joints can be found
152 in the literature [48]. The disadvantage here is that the larger the size in the direction of optical axis, the more complex its
153 design and manufacturing turns out to be [49].

154 **3.2.2 Optical element kept in place by a free sitting clamp**



155
156 **Figure 4. Four-stroke optical engine, the rectangular window is sandwiched by the clamp and soft gaskets [6, 7].**

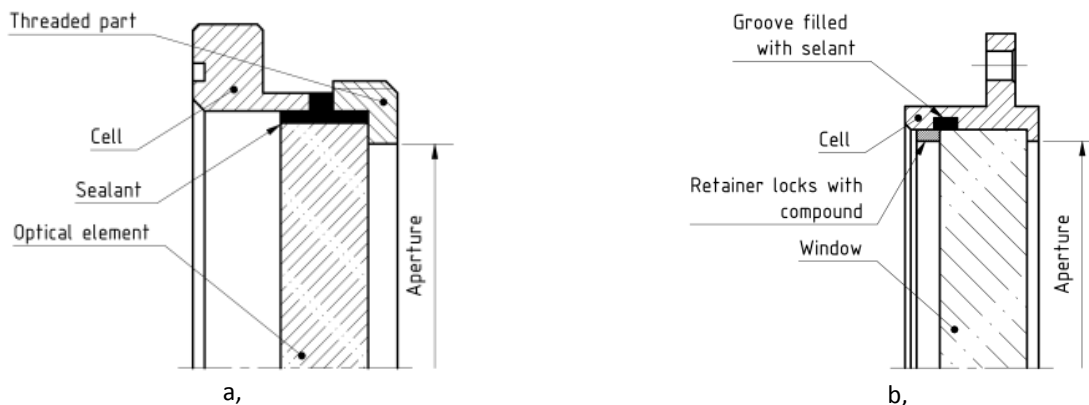


157
158 **Figure 5. Special sodium chloride free sitting window for a high-temperature, high pressure difference, IR spectra [50]**

159 The simplest design solution is illustrated in Figure 4 and Figure 5. The clamp is not guided but constrained by contact in one
160 one axis and constrained by friction along the other two axes; its position is defined by fixing bolts. Its advantages are: a simpler
161 design, easier to manufacture, smaller in size along the optical axis, and that its position along the optical axis can easily be
162 varied. Its disadvantage is that a greater amount of mechanical (bending) load on bolts is required; since the window can
163 freely move, bringing the assembly together can also be problematic.

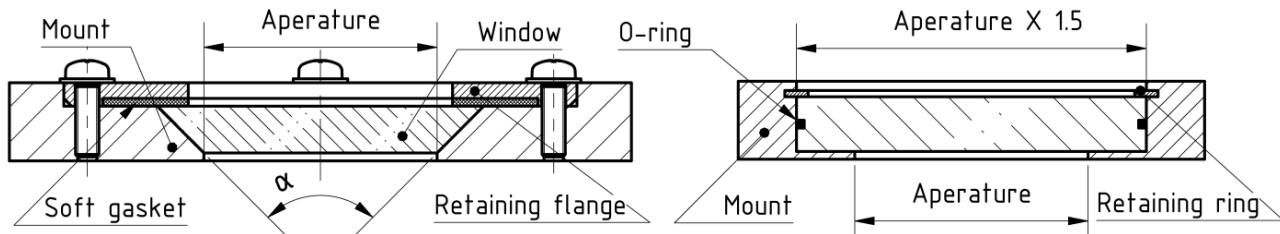
164 **3.2.3 Adhesives**

165 Fixing an optical element in a carrier frame using adhesives, as indicated in Figure 6 is a convenient solution for lower
166 pressure and temperature environments. In both cases, the window sits against a shoulder which provides an accurate
167 positioning. All mechanical loads rising from the pressure differential are taken by the adhesive. In the second case, the
168 adhesive acts as a sealant and retainer; only, the stress is induced, but the pressure difference is taken by the shoulder on
169 the frame cell. The main advantage of this solution is the modest space requirement. Its only disadvantage is that the
170 performance of the assembly is proportionately dependent on the properties of the adhesive, which are usually limited.



171 **Figure 6. a, Using adhesives for a low pressure application [51]; b, Using adhesives for a moderate pressure application [52].**

172 **3.2.4 Fitted inside the shell of the vessel**



173
174

Figure 7. Window integrated in the vessel body [53, 54].

175 The optical element can be fitted inside the housing, a typical application area is the deep submergence vehicles, Figure 7.
176 There is no need for bolts as the major load-bearing element. Its advantage is that this setup can take large pressure
177 differences, while the vessel geometry can also be made more simply. Its disadvantage is that the window can only be
178 dismantled from the pressurised side, more complex window geometry required.

179 **3.3 Structural design and performance**

180 **3.3.1 Allowable or design stress in the optical element, safety factor**

181 The estimation of the allowable or design stress is among the most important and sometimes challenging tasks, especially
182 at elevated temperatures [23-25, 55-57]. The data of mechanical properties can be found in the literature for the more
183 common materials; however, there often is no consistency in the given values. It becomes even more difficult to find
184 information when practical issues are being considered, such as the effects of temperature, humidity, manufacturing
185 technology, surface finish, and loading rate. Pressure vessel codes provide suggestions for high strength alloys which can
186 then be taken as a first guidance for optical materials. According to BS EN 13445-3 [56] and ASME Boiler and Pressure Vessel
187 Code Section VIII [57], the design stress should be calculated as:

188 (EN)
$$\sigma_{des} = \min\left(\frac{R_{p0,2/T}}{SF}; \frac{R_m/20}{SF}\right) = \min\left(\frac{R_{p0,2/T}}{1,5}; \frac{R_m/20}{2,4}\right) \quad (1)$$

189 (ASME)
$$\sigma_{des} = \min\left(\frac{R_{p0,2/T}}{SF}; \frac{R_m/20}{SF}\right) = \min\left(\frac{R_{p0,2/T}}{1,5}; \frac{R_m/20}{2,14}\right) \quad (2)$$

190 where, σ_{des} is the allowable design stress; SF is the safety factor; $R_{p0,2/t}$ is the 0,2% proof strength at T temperature; R_m is
191 the tensile strength at 20 °C [58]. As optical materials discussed in this work have brittle characteristics, it is only the safety
192 factors that are associated with the tensile strength that are applicable. It is suggested that the safety factor for optical
193 design should always exceed 2. The general value for a well-designed system is around 3, when failure is not expected to
194 cause major damage. When there is more uncertainty in the design, the usual and conservative safety factor value is 4. The
value can be as high as 5 for non-optimum or unplanned conditions (manufacturing or usage) or when failure can cause
significant damage [51, 59].

195 **3.3.2 Geometric and mechanical tolerances**

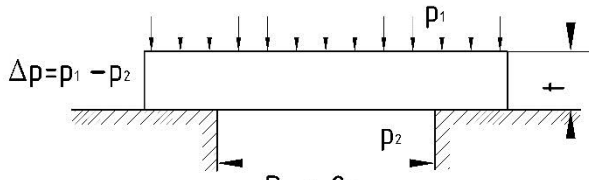
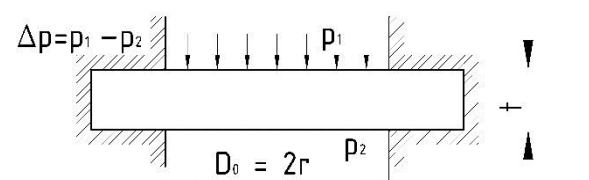
196 The tolerances on diameters and on the thickness of the centre and edges are comparable to general precision
197 manufacturing, typically h6 to h11. When the edge of the window is not fitted and/or it is not a sealing surface the size
198 tolerance is in the 0.1-0.01 mm range. The tolerance on the thickness of the optical access has importance for lenses but for
199 windows it is not crucial. Similarly, the usual parallelism requirements are on the fine side but are comparable but to the
200 ones used in pressure vessel manufacturing. However, the surface roughness values are in a couple of order less than the
201 typical values for precision manufacturing technologies for metals. Moreover, the quality of the finish is further described
202 by the scratch and dig number. A usual scratch/dig specification consists of two numbers e.g. 80/50. The first number
203 indicates the maximum size of cracks (scratches) on the surface of the optical element. The second number describes the
204 maximum size of round-shaped imperfections: digs and pits [60, 61].

205 Guidelines are given in Table 3 for selecting optical and mechanical properties for sight window applications.

206 **3.3.3 Deflection and stress**

207 Equations relating deflection to the applied pressure difference can be found in the literature for a number of shapes and
208 support modes [62, 63]. In this work only the details of relations for the plane-parallel circular window shape are shown.

Table 2, Classical mechanics of plane-parallel circular elements

Non supported case	Supported case
	
$\delta = \frac{3(3 + \mu) \Delta p r^2}{8 t^2} = K_w \frac{\Delta p r^2}{t^2} \quad (3)$	$\delta = \frac{3 \Delta p r^2}{4 t^2} = K_w \frac{\Delta p r^2}{t^2} \quad (4)$
$K_w = 0.125 \quad (5)$	$K_w = 0.75 \quad (6)$
$x = \frac{3}{16} (-\mu^2 - 4\mu + 5) \frac{\Delta p r^4}{E t^3} = K_x \frac{\Delta p r^4}{E t^3} \quad (7)$	$x = \frac{3}{16} (1 - \mu^2) \frac{\Delta p r^4}{E t^3} = K_x \frac{\Delta p r^4}{E t^3} \quad (8)$
$K_x = 0.96 \quad (9)$	$K_x = 0.17 \quad (10)$

209

210 K_w is a generalised constant suggested by textbooks [51, 52, 59]. In these works, K_w is chosen conservatively to cover a
 211 wide range of optical materials. This conservative method was chosen in this study to make a suggestion for values of K_x .
 212 In the rest of the equations, (3)-(10) δ is the stress; μ is the Poisson ratio; Δp is the pressure differential; r is the radius
 213 which is half of the aperture or diameter D_0 ; x is the deflection; t is the thickness of the optical element; E is Young's
 214 modulus. If the the stress equations are rearranged and the safety factor, the diameter and design stress are inserted, then
 215 the minimum required thickness of the optical element can be calculated.

$$t_{min} = \left(\frac{1}{2} D_0 \right) \left[\frac{K_w S F_\delta \Delta p}{\sigma_{des}} \right]^{1/2} \quad (11)$$

216 where, t_{min} is the minimum thickness of the circular optical element; D_0 is the diameter of the aperture; $S F_\delta$ is the safety
 217 factor; Δp is the applied pressure difference on the optical element; σ_{des} is the allowable design stress. Using Equations (7)
 218 and (8), the deflection can be calculated or the rearranged version with the maximum allowable deflection can be used to
 219 find the minimum required thickness:

$$t_{min} = \left[\frac{S F_x K_x \Delta p D_0^4}{16 E x_{max}} \right]^{1/3} \quad (12)$$

220 where $S F_x$ is the safety factor. In general, as $S F_\delta$ is associated with complete breakdown and failure and $S F_x$ has an effect
 221 on only the quality of the image produced by the optical element. $S F_x$ can have a significantly lower value than the $S F_\delta$.
 222 Equation (12) provides results for a simple case of a mechanical load. When, there is a combined load from thermal and
 223 mechanical loads, the deflection needs to be calculated using Finite Element Analysis (FEA). The result of the simulation can
 224 be used to calculate the outer radius (R) of the window that can be turned into a divergent meniscus lens (assuming the
 225 same deflection on both sides of the window):

$$R = \frac{x^2 + D_0^2}{8x} \quad (13)$$

226 Then with the known thickness the lens power (P_{lens}) can be calculated:

$$P_{lens} = (n - 1) \frac{-t}{R^2 - Rt} \quad (14)$$

227 The maximum deflection of a window is a function of allowable image distortion. In an optical system with lens and sensor,
 228 the lens focusing error usually gives the tolerance in dioptres. It is hard to find tolerances published, but as a rule of thumb
 229 some values are summarised in Table 3, [64-67].

230 Equations of stress, deflection and power calculation for rectangular, plan parallel windows can be found in [68].

231 3.3.4 Failure estimation by statistical tool

232 It is a common practice to implement Weibull statistics to estimate the probability of failure (P_f) when a given σ load is
 233 applied on a brittle material.

$$P_f = 1 - \exp\left[-\left(\frac{\sigma}{\sigma_0}\right)^m\right] \quad (15)$$

234 where m is a constant describing the variability in strength; their values having been experimentally determined and
 235 published. σ_0 is a stress level at which 63% of the samples fail, m is the so called Weibull modulus and indicates the scatter
 236 of fracture stress around σ_0 [51, 69-72]. The acceptable values can differ significantly and they should be determined for
 237 each application individually. Some suggested examples: for a cheap easily replaceable cutting tool - 10^{-2} ; for an expensive
 238 part that upon failure can cause serious damage - 10^{-4} ; when personal injury is at risk - 10^{-6} ; when the outcome of a failure
 239 could be fatal then 10^{-8} .

240 3.4 Optical design and performance

241 3.4.1 Birefringence and maximum optical path difference (OPD)

242 It is usual for most practical optical materials to have two indices of refractions. Their refractive index is a function of the
 243 propagation-direction and polarisation of the incident electro-magnetic wave. Furthermore, it is a function of the
 244 mechanical stress in the medium. Optical substances having this property are called birefringent materials [73]. The level of
 245 birefringence is expressed as a difference in the optical path of two perpendicular states of the polarised wave. This
 246 inequality in distance is called the OPD and it is measured in nanometres. The OPD has been previously investigated for
 247 plane-parallel circular plates with a pressure differential applied on them; Sparks et al. [74] derived an approximate relation:

$$\text{OPD} = 8.89 \times 10^{-3}(n - 1) \frac{\Delta p^2 D^6}{E^2 t^5} \quad (16)$$

248 where, OPD is the optical path difference; n is the refractive index of the material; Δp is the pressure difference applied
 249 across the planes of the optical element; D is the aperture, the unsupported diameter of the optical element; E is Young's
 250 modulus of the medium; and t is the thickness of the window. This OPD caused by an applied stress called the stress
 251 birefringence. It is measured as OPD per unit travel path; its unit is nm/cm. The details of the maximum allowable tolerances
 252 on birefringence for some applications are given in ISO 10110-8 [61] and Kimmel and Parks [75]; a summary is presented in
 253 Table 1. Equation (16) can be rearranged to find the minimal required thickness:

$$t_{\min |ODP\Delta p} = \sqrt[5]{8.89 \times 10^{-3}(n - 1) \frac{\Delta p^2 D^6}{\text{OPD} \cdot E^2}} \quad (17)$$

254

Table 3. Sight window properties for different applications

Precision	Typical application	Maximum power of a deflected window (diopetre)	Maximum OPD per unit path length (nm/cm)	Parallelism or plane angle (degree)	Flatness (λ is the characteristic wavelength)	Surface finish or roughness (nm)	Surface finish quality
Extreme	Polarisation and interference instrumentation, deep-space instrumentation	No data	2	No data	$\frac{\lambda}{20}$ or better	0.3	No data
High	Photolithography optics and astronomical telescopes	No data	5	0.001	$\frac{\lambda}{10}$	0.5	10/5
Good	Photographic and microscope optics, visual telescope	$10^{-2} - 10^{-6}$ *	10	0.01-0.001	$\frac{\lambda}{2} - \frac{\lambda}{4}$	1	40/20-20/10
Semi	Eyepieces, viewfinders, magnifying glasses	10^{-1}	20	0.1-0.01	λ	2	60/40
Commercial	Illumination optics, condenser lenses	No req.**	No req.	0.1	No req. - 2λ	4	80/50

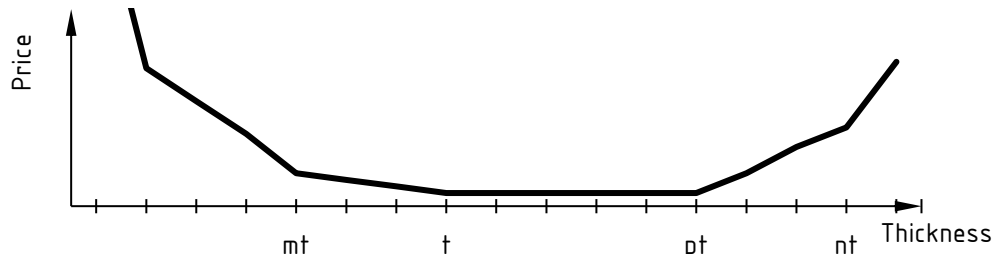
*in general it can be said that, tolerance values in the order of 10^{-6} or less are likely to be negligible when they are compared to the uncertainty in the focus adjustment of a lens system
 ** No req.: No requirement

255 It is important to note that there are always some residual stresses in optical materials, depending on the quality of the
 256 manufacturing processes. More details relating the manufacturing process to stress birefringence can be found in the
 257 references.

258 **3.4.2 Factors limiting the maximum thickness**

- 259 • The most obvious limiting factor is the available space the geometric constraints, which depends on the individual
 260 design. The different possible mounting methods and previous publications of solutions are introduced in other
 261 sections of this work.
- 262 • Transmittance change as a function of material thickness [27]. Significant decrease of the transmittance can only
 263 occur with large thicknesses, this is not a usual design constraint for high load applications.
- 264 • Temperature gradients can cause stress concentration in window materials. For heated or cooled designs this can
 265 limit the size of the geometry. Ceramics with larger thermal conductivity coefficients are less sensitive to thermal
 266 shock, [76, 77].
- 267 • Price: manufacturing and material cost
 268 As Figure 8 indicates typically there is a thickness range where the price is at its minimum. This is the most
 269 commonly made size range ($t \leftrightarrow pt; p \sim 3 \dots 5$) that is mass produced with a variety of tolerances and finishes.
 270 These are usually used in general optics and not adequate for high load applications. To the left from this region
 271 ($t \leftrightarrow mt; m \sim 0.6 \dots 1.0$) there is an increase in price where the manufacturing becomes more laborious. The
 272 relatively thin geometry makes the window fragile and prone to deflection under the manufacturing loads. A
 273 further sharp rise expected for thicknesses below mt where extra care is required to provide precision finish. For
 274 example, during manufacturing there is a 50% breakage rate for 0.2mm borosilicate glass coverslips. On the right
 275 hand side from the flat ($pt \leftrightarrow nt; n \sim \text{few hundreds}$) the increase is driven by the cost of material. nt represents

276 the maximum size that is achievable using the standard or already existing raw material production tooling. Larger
277 geometries can only be made if tooling cost is covered.
278 Figure 8 only introduces general trends in the price the actual values will differ from geographic region to region,
279 material type, and quantity required.



280

281

Figure 8. Approximate cost of manufacturing of disc-shaped windows as function of thickness

282

3.4.3 Other design considerations

283

In this section further design considerations are listed and referenced. They are not of interest to this study, but they can be potentially important for other designs, for instance, in applications where the pressurised chamber is used with high accuracy polarisation or interference instruments or deep space applications.

284

285

286

287

288

289

290

- Compressive stress caused by sharp edges on the surface of an optical element [78, 79]
- Effect of a temperature gradient on adhesive bonds [52, 80]
- The tensile stress in a brittle material due to a compressive load on its surface [52, 63, 81]
- Focus shift in thick parallel plane optical elements [82]
- Distortion caused by a temperature gradient [71, 83-85]

291

4 Design of an optically accessible pressure chamber

292

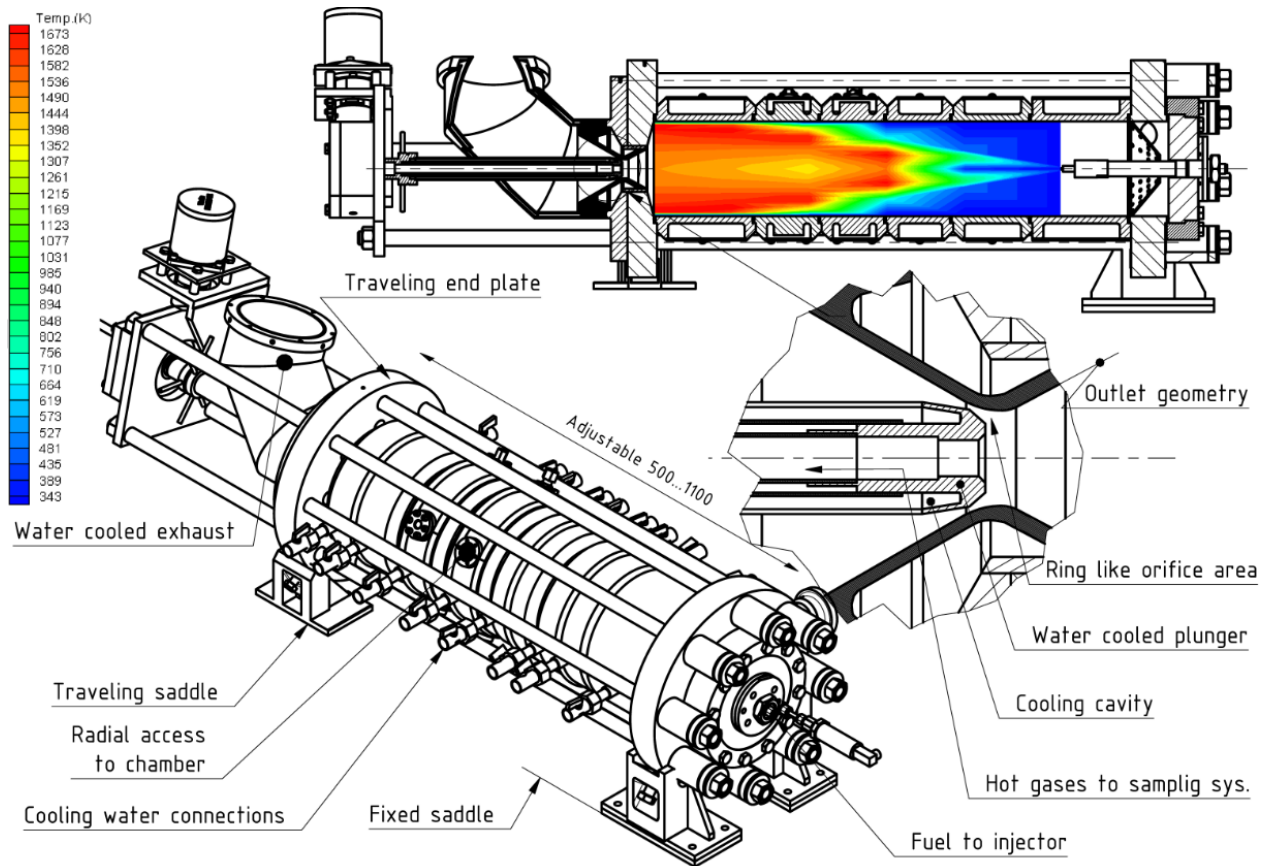
293

294

295

296

The detailed geometry of the existing combustor is shown in Figure 9. An important feature of it is that the working chamber was constructed from sections. Utilising this property, the reactor's length could be varied to adjust the residence time of the reactants. Different length sections were available to build the reactor. When the reactor was assembled, the sections were sealed by polymer O-rings. As a result of the limited temperature resistance of the stainless steel structure and the high thermal load, the sections had to be individually water-cooled, as in Figure 9.



297

298

299

300

Figure 9. An isometric and a section view of existing chamber, computational result of in-cylinder temperature distribution shown in the section view. Conditions: diesel fuel; stoichiometric ratio; 6 bar in-reactor pressure.

301

4.1 The section

302

4.1.1 Design requirements

303

304

305

306

307

308

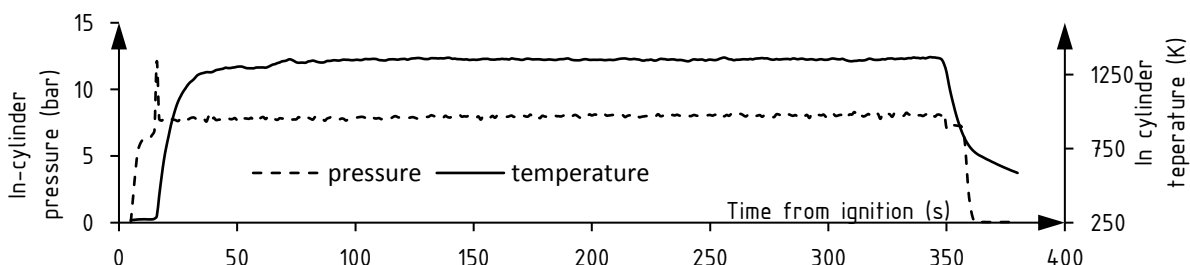
309

310

311

312

It was required that the optical section withstand the maximum of 20 bar working pressure at the maximum possible operating temperature and that its geometry would allow it to be connected it to the existing rig. In order to seal the reactor, it was essential to maintain the temperature at an acceptable level in the O-ring grooves. The maximum continuous operating temperature of the Viton O-rings (200 °C) was chosen as a limit on the surfaces that were in contact with the rings. The system could provide a maximum cooling flow rate of 10 litres per minute for the new optical section. The highest allowed inflow cooling temperature was 70 °C. The estimation of the heat flux coming from the combustion to the section was based on a number of test results where an in-chamber, single-point gas temperature measurement was taken. An example of these results is shown in Figure 10. The results of computational work on combustion and in-chamber conditions by Demosthenous and Crookes [10] were used as input boundary conditions for the analysis, Figure 9. It was also a requirement that the windows could be easily changed to metal blanks for heating up or non-optical tests.



313

314

315

Figure 10. Typical test results of the existing combustion chamber; the time of ignition is indicated by the rapid increase in temperature and a pressure peak at around 10s after ignition

316

317

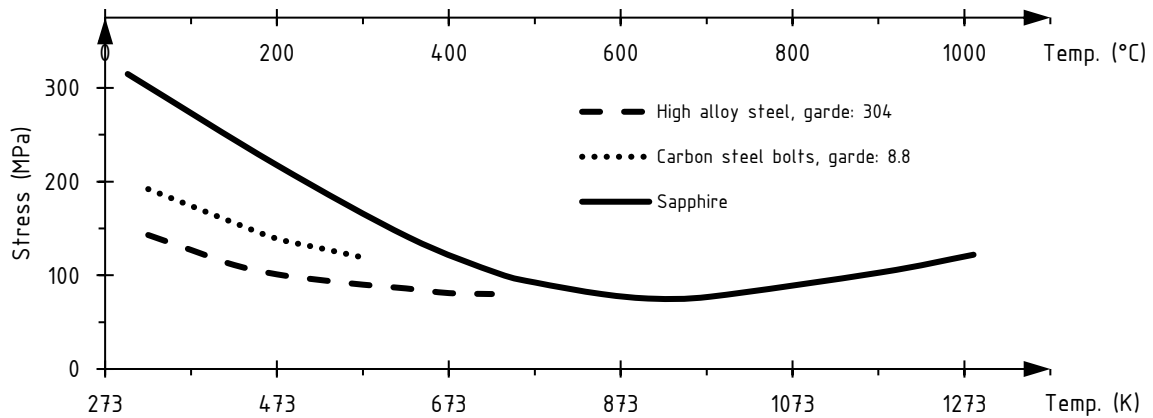
318

It was an underlying requirement that the new apparatus would allow investigation with a Phantom 4.3 high speed camera, a TSI Particle image velocimetry system (laser: dual 50 mJ/pulse, NewWave Gemini Nd:YAG; sensor: PowerView 4MP) and a FLIR Titanium 560M infrared (IR) camera.

319 **4.1.2 Material choice**

320 As shown in Figure 12, the resultant optical section is a complex shape, featuring fine finished surfaces for sealing purposes.
321 It is thus that the material of the section body needed to have adequate strength to withstand the pressure load at high
322 temperatures. It also needed to be suitable for precision subtractive and additive manufacturing. Moreover, due to the
323 corrosive products forming inside the chamber and the constant presence of cooling water, the material was required to
324 have some corrosion-resistant properties. A detailed list of possible materials can be found in EN134453 [86]. The
325 aforementioned requirements suggested using an austenitic stainless steel grade. After considering the cost, the corrosion
326 resistance and manufacturability grade 304 (1.403) was chosen. It is easily available, with well-documented data on its
327 mechanical properties at elevated temperatures showing the tensile stress for the materials that were used to construct
328 the optical combustor, Figure 11.

329 The material selection procedure for the combustor body and for the optical element was based on general guidelines with
330 practicality and availability in focus. However, in design tasks where material cost or other material attributes have higher
331 significance more detailed material selection methods could be employed, as described in [87, 88].



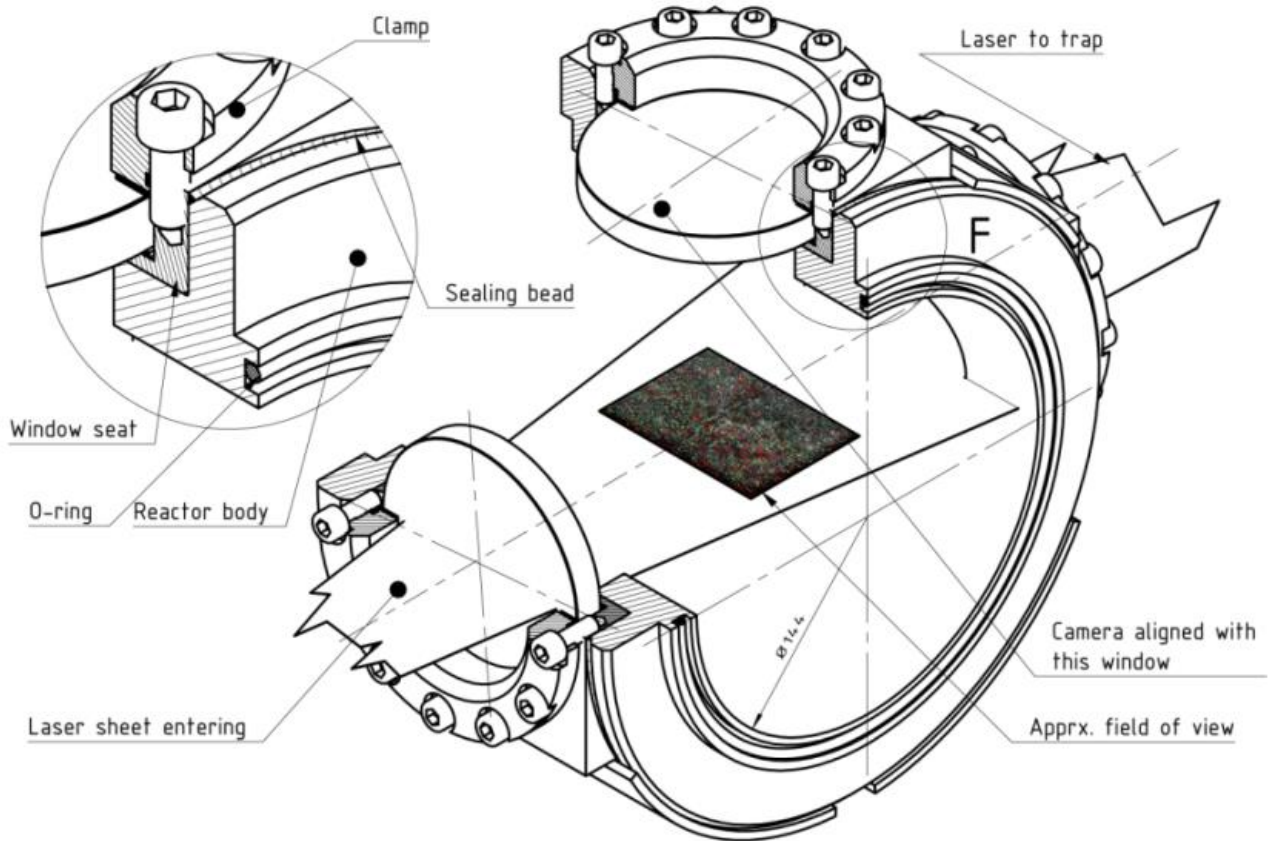
332

333

Figure 11. Permissible design stresses of some selected materials as function of temperature [37, 56].

334 **4.1.3 Design of required geometry and validation**

335 This structure of the overall design defined some underlying properties of the optical access. It was the obvious choice that
336 the optical access should be constructed on a section which has similar dimensions and had the same sealing method. Given
337 the nature of the laser-radiation-based measurement method, a three-access point – in a T-like configuration – was
338 required. A detailed review of optical measurements can be found in the books by Zhao [12, 13]; see details in Figure 12.
339 This three-access point design was satisfactory for the high speed and IR camera setup.



340

341

Figure 12. The final design of the optical section. The laser sheet entering and leaving the chamber is also indicated.

342

343

344

345

346

347

At its maximum performance the HPC burns approximately 4 g/s Diesel fuel; it can be seen that cooling is essential for the continuous operation of this reactor. Insufficient cooling would result in a rapid increase of temperature in the body and in the window (or blank). The excessive thermal load could lead to the quick failure of the polymer seals. Therefore, the geometry of the body with window seats had to provide enough surface area for the coolant and allow sufficient volume flow. Assuming the largest heat flux and inflow cooling temperature, a number of simulations were carried out to estimate the temperature distribution of solids and the coolant.

348

349

350

351

Full three-dimensional numerical model was implemented in SolidWorks Multiphysics modelling package using finite element method. Linear tetrahedral 4-nodes elements were used to discretise the solid components for the structural analysis whilst hexahedral cells were adopted for the fluid dynamics. The number of cells for the solid and fluid subdomains were 94710 and 62174 respectively, from which 66683 solid cells were in contact with the fluid.

352

353

354

355

356

357

358

For the purpose of structural analysis, a fixed constraint was applied on the connecting surfaces at one side and an axial evenly distribute load was added on the relevant surfaces other end of the section. Finally, a pressure load of 2 MPa was applied on the internal surfaces. The flow analysis was defined by setting the temperatures, pressures and mass flow rates for the cooling flow and hot air inside at the inlet and outlet boundaries. The mesh and grid independence was investigated by means of software embedded tools where the mesh and grid were refined taking the notch effect, stress concentration and thermal singularities into account. Once the model was set up the coolant flow rate was varied and the temperatures were monitored, especially the temperature of the O-ring groove as shown in Figure 15 b.

359

360

361

362

The validation of the model was carried out experimentally. The temperatures of the coolant entering and leaving the section was measured and recorded. Moreover, the outside surface temperature of the metal blanks was monitored for validation purposes. It was found that the difference between the temperature values predicted by the numerical model and measurements was approximately 15%.

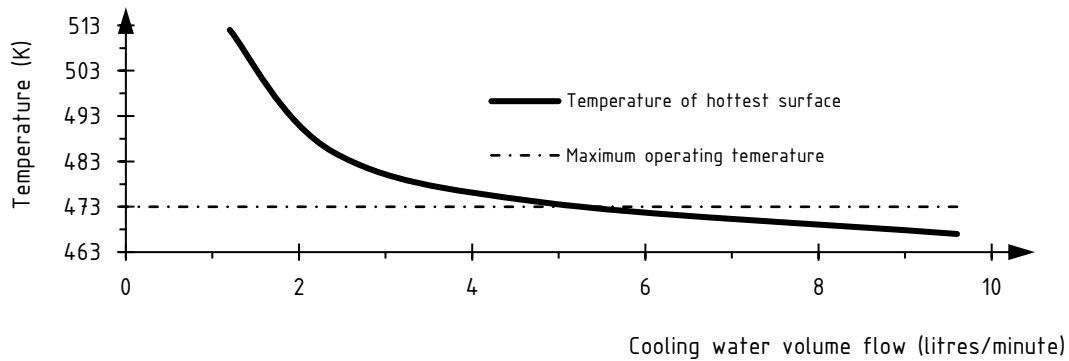
363

364

365

366

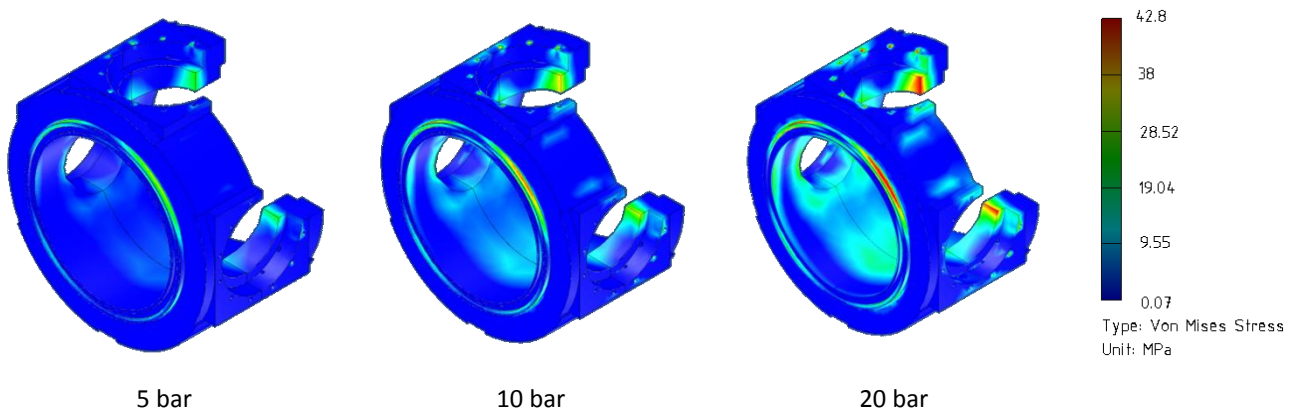
The O-ring groove temperature curve was plotted against the coolant flow rate, Figure 13. It was found that having at least 5.5 litres per minute coolant flow rate on the designed geometry could keep the O-ring groove temperature at an acceptable level. The 5.5 litres per minute minimum cooling flow requirement is below the 10 litres per minute maximum performance, therefore the given cooling system was found to be sufficient.



367

368 **Figure 13. The O-ring groove temperature as the function of the coolant volume flow (value was taken from the corner**
 369 **point of the hottest possible cross section, as indicated in Figure 15b).**

370 The length of the section was chosen to be the same as that of the longest existing section. The thickness of the optical
 371 section was based on the existing design. Polymer O-rings were used to seal between the sections, the design and
 372 manufacturing were according to BS ISO 3601 [89]. With the given length, a circular window type was selected for easier
 373 machining and the geometrically maximum possible diameter, 82 mm, was chosen to be evaluated. FEA was carried out to
 374 determine the stress arising from thermal loads and applied pressure. As is indicated in Figure 14, the highest stresses are
 375 in the O-ring grooves and in the openings. The grooves had high stresses on their contact surfaces because of the large axial
 376 force pressing the sections together against the pressure. In the case of the openings the high stress rate can be explained
 377 by the reduced material volume, i.e. reduced inertia [90].



378

Figure 14. Stress distribution as a function of chamber pressure

379 The inner diameter of the optical section is 144 mm; the outer diameter is constrained by the support rods, as seen in Figure
 380 9. As the radial space was limited, the best design solution would have been to place the optical element inside the shell –
 381 but with the given casted base, this was not achievable. Therefore, the second best option – with an eye to optimising
 382 storage space – was to have a free sitting clamp; this setup is shown in Figure 12. The detailed section-view shows the
 383 window kept in place by the circular clamp. The clamps were fixed and positioned by 12 M6 socket-head bolts to the window
 384 seats. The window seats were welded all around to the base chamber or reactor body; the beads sealed the seats and kept
 385 them in place. The window to seat-sealing surfaces were precision-manufactured, as suggested in PD5550:2009 Table 3.8-
 386 3 [91]. With the aid of the measurements and computational results, further analysis was carried out to estimate the working
 387 temperature of the section and optical elements. The temperature distribution of the cross-sections is shown in Figure 15.

388 4.2 The optical access

389 In this section the design process of a plan parallel circular optical element is introduced via a case study. Table 4 simplifies
 390 the procedure into four main steps showing all the properties that have effect on the design. In the following subsections a
 391 practical application of Table 4 is presented. The values for the variables and main functions/relations are cross-referenced
 392 from Section 3.

Table 4. Summary of input variables and their use during the design process of a plan parallel optical element

1, Determining design specifications:	<p>Collection of information that is required to carry out the design task.</p> <p>Instrumentational requirements</p> <ul style="list-style-type: none"> •EM range /Sensor responsivity (nm) •Transmissivity (%) •Window aperture (mm) <p>Nature of application, precision</p> <ul style="list-style-type: none"> •Power from deflection (diopetre) •ODP (nm/cm) •Parallelism (degree) •Flatness (fraction of characteristic wave length) •Surface finish (nm) •Surface quality •Properties of thermal and mechanical loads •Chemical environment •Safety factor <p>Geometric requirements</p> <ul style="list-style-type: none"> •Constrains in all directions (mm) •Window aperture (mm) •Sealing surface area and shape
2, Material selection:	<p>This task can be carried out considering the following material properties</p> <ul style="list-style-type: none"> •EM range (nm) •Transmissivity (%) •Compatibility with environment •Availability
3, Thickness determination	<p>Calculation of the minimum thickness:</p> <p>This a usual undertaking where the minimum amount of material is determined that still ensures the window performing without any failure. Numerical methods can be used to decrease the uncertainties in the result.</p> <ul style="list-style-type: none"> •Structural analysis, maximum stress (MPa) •ODP (nm/cm) •Power from deflection (diopetre) •Probability of failure <p>Maximum thickness:</p> <p>The maximum window size is restricted by the followings.</p> <ul style="list-style-type: none"> •Constrains in all directions (mm) •Transmissivity (%) •Cost constrain
4, Manufacturing details and instructions	<p>The tolerances and finish of an optical element depends on the application and precision required. The overall size is a result of the thickness determination and geometric constraints.</p> <ul style="list-style-type: none"> •Geometry: aperture, sealing area, diameter, thickness •Tolerances •Parallelism (degree) •Flatness (fraction of characteristic wave length) •Surface finish (nm) •Surface quality

4.2.1 Determining design specification

395 The main purpose of the window is to provide a transparent barrier between the combustion and instrumentation. An
396 underlying requirement was to allow use of three different sensors (cameras) with differing spectral responses. Wavelengths
397 of interest are particulate imaging velocimetry (around 532 nm), high speed camera (visible spectra) and IR camera (3 to 5
398 micron); the responsivity curves are shown in Figure 2. As the wavelength of the laser is in the visible range, there were two
399 bands of electromagnetic radiation that needed to be considered – 380-985 and 2800-5200 nm. In these regions, the
400

401 minimum of 80% transmittance was required. The tolerance on the OPD had to be kept in the photographic range: 10
 402 nm/cm. As the three sensors were robust and the measurements by them were not overly sensitive, the maximum allowed
 403 lens power of the distorted window was 10^{-6} dioptre. The maximum expected pressure difference on the optical element
 404 was 20 bar. The required safety factor was required to be four for stresses arising from mechanical and thermal loads, with
 405 a maximum probability failure of 10^{-4} . The technological considerations and tolerances were chosen to fit laser and the
 406 precision measurements requirements. The level of precision was selected to be good according to Table 3. Finally, the
 407 operating temperature of the window had to stay under the maximum permitted level.

408 **4.2.2 Material selection: transmissivity and environmental requirements**

409 The spectral requirement is shown in Figure 2 along with the transmittance curves. The ideal design solution was to select
 410 only one material type to cover the required wavelength ranges. It can be seen that the two possible material types that
 411 cover the needed large range of EM wavelengths are sapphire and magnesium fluoride. The thermal analysis of the optical
 412 section indicated that the steel blanks and windows would need cooling to survive. The calculations and simulations were
 413 carried out for both materials. It was found that MgF_2 can be a valid option for low-temperature and low-humidity
 414 environments. Extra caution is required when a temperature gradient is applied on the MgF_2 material, as its high expansion
 415 coefficient and middle-range conductivity combined with low strength makes it sensitive to thermal shock. It is also
 416 suggested by manufacturers that MgF_2 can react with high temperature steam similar to the one that can be found in the
 417 HPC as a combustion product. Therefore, sapphire was, instead, chosen as material for the windows as it combines good
 418 transmittance in all the required wavelength bands as well as having good thermo-mechanical strength.

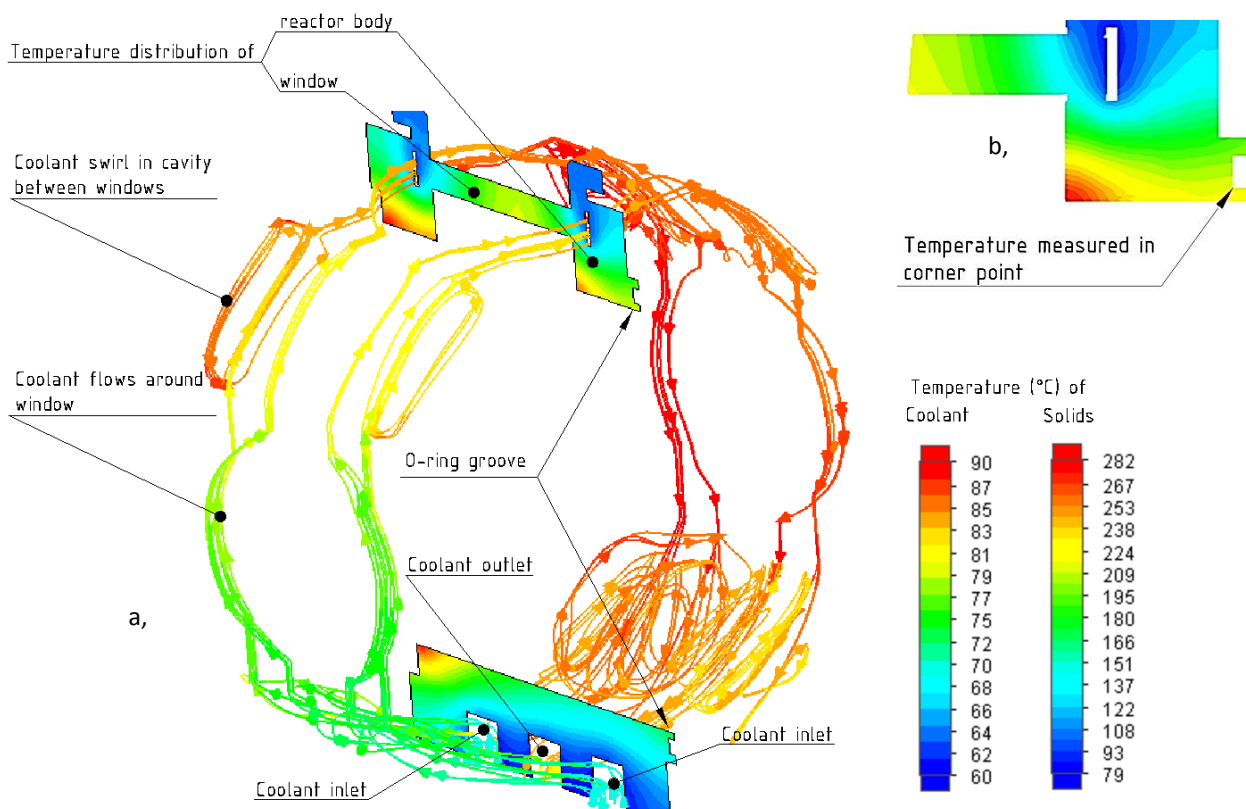


Figure 15. a) An isometric view of the flow of cooling water, its temperature change and the temperature distribution of a cross section of the reactor. b) Temperature distribution around the O-ring groove.

419 **4.2.3 Determination of required thickness and validation**

420 The diameter of the window was determined by the maximum available space in the optical section. The maximum possible
 421 diameter was found to be 82 mm. Previous experience showed that a width of 9 mm minimum contact surface is required
 422 to provide an adequate sealing performance. The 9 mm wide contact ring also ensured an acceptable level of compressive
 423 stress in the window and provided large enough heat transfer surface for the metal blanks. This geometric design resulted
 424 in a 64 mm aperture. The thickness of the window was estimated by using the equations and relations that were explained
 425 earlier in this paper, and then validated by FEA. The minimum thickness was calculated for two requirements: maximum
 426 allowable stress and OPD. Substituting values to Equations (11) and (17) the thickness value results were 5.88 and 0.07 mm
 427 respectively.

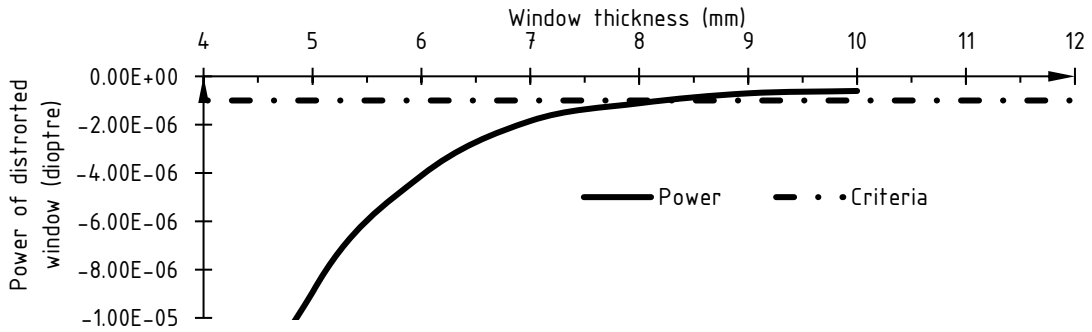
$$t_{min|\delta} = \left(\frac{1}{2}D_o\right) \left[\frac{K_w SF_\delta \Delta p}{\delta_{des}}\right]^{1/2} = \left(\frac{1}{2}64\text{mm}\right) \left[\frac{0.75 \cdot 4 \cdot 2\text{MPa}}{178\text{MPa}}\right]^{1/2} = 5.88\text{mm} \quad (18)$$

$$t_{min|ODP\Delta p} = \sqrt[5]{8.89 \cdot 10^{-3}(n-1) \frac{\Delta p^2 D^6}{OPD \cdot E^2}} = \sqrt[5]{8.89 \cdot 10^{-3}(1.76-1) \frac{(2\text{MPa})^2 \cdot (64\text{mm})^6}{10 \frac{\text{mm}}{\text{cm}} (345\text{GPa})^2}} = 0.07\text{mm} \quad (19)$$

428 The results of the estimation indicated that, with the given loads and geometry, the required optical performance was easily
 429 achievable. Then, the window deflection was calculated using FEA for the highest thermal and mechanical loads. The stress
 430 and deflection results were substituted in Equations (13), (14) and (15) in order to check the design for failure probability
 431 and image distortion. Equations (13) and (14) combined together gives the power of a distorted window as function of
 432 refractive index, aperture and deflection.

$$P_{lens} = \frac{64(n-1)tx_{(t)}^2}{(D_0^2 + x_{(t)}^2)(D_0^2 + x_{(t)}(x_{(t)} - 8t))} \quad (20)$$

433 The power as function of window thickness for the given geometry is shown in Figure 16.



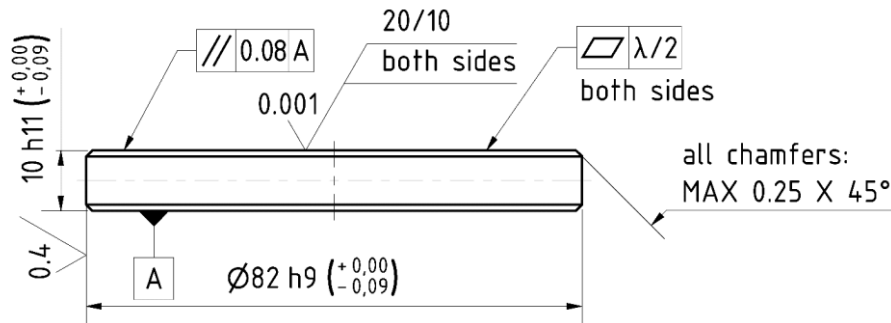
434
435 **Figure 16. Power of distortion vs window thickness**

436 It was found that the limiting factors were the probability failure and deflection. Based, on the curve above and financial
 437 consideration the thickness was chosen to be 10mm. Using FEA, the maximum stress was found to be 42.8MPa, with this
 438 level of stress:

$$P_f = 1 - \exp\left[-\left(\frac{\sigma}{\sigma_0}\right)^m\right] = 1 - \exp\left[-\left(\frac{42.8\text{MPa}}{485\text{MPa}}\right)^5\right] = 5.35 \cdot 10^{-6} \quad (21)$$

439 It is likely that there is a high inaccuracy in this result of probability failure. The value of σ_0 is function of a number of
 440 variables, one of the most important ones is temperature. In the equation above the value for σ_0 corresponds to room
 441 temperature, and its value expected to be show high sensitivity to changes in temperatures and therefore the probability
 442 failure result can only be received as a guideline. However, no data available for σ_0 in the literature for elevated
 443 temperatures

444 4.2.4 Results and detailed design



445
446 **Figure 17. Side view: final sapphire sight window design, where $\lambda = 532\text{nm}$**

448 Figure 17 shows the final and detailed manufacturing instructions of the sapphire window. The material selection,
 449 calculation of geometries and tolerances specified were carried out according to Table 4. The stainless section was
 450 manufactured in-house and three sapphire windows were purchased from a specialist company. These were installed in the

451 section to make the optically accessible combustor as shown in Figure 12. The HPC with the optical access has been fired
452 and fully tested successfully. The rig is capable to give insight to the high-pressure combustion process, providing optical
453 data at different EM wavelengths. Figure 18 indicates the results gained from the working optical section using different
454 instrumentation.

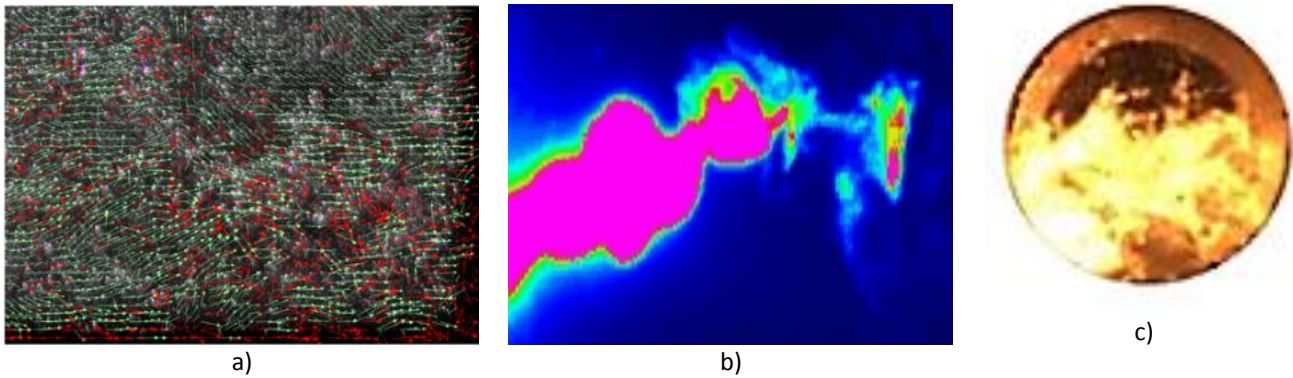


Figure 18. Results from the optical HPC: a) PIV vector field of the flowing air fuel mixture, laser measurement. b) IR radiation image recorded from a hydrocarbon flame. c) A still image from high speed video, visible spectra.

455 **5 Conclusion**

456 This work has investigated the design of pressure vessels equipped with optical access. A significant number of data sources
457 were surveyed to produce a comprehensive review of the most related optical, thermal and mechanical properties for some
458 optical materials. The database was presented in a way that allows for a convenient and direct comparison. It was concluded
459 that larger safety factor values are required for optical element design, typically ranging from two to five depending on
460 operating conditions, manufacturing technology, risks and hazards and so on. The safety factor selection procedure and
461 criteria was clearly described. The high values suggested is the result of the inconsistency found in available data sourced
462 from suppliers and from the literature of the thermal and mechanical properties of optical materials.

463 The little design criteria that was available on the topic in the literature was presented, while also considering practical,
464 mechanical and optical design considerations. The aspects of the design for optical performance were described in-depth,
465 with additions to the already published equations and relations. The utilisation of this database allowed for the design
466 process of a pressure chamber, with optical element under high mechanical and thermal load, to be demonstrated, where,
467 the required experimental rig needed to support research activity for a range of optical instrumentation.

468 **6 Acknowledgement**

469 The modelling and simulations were carried out with SolidWorks under an academic licence. This research project was
470 supported by the Central Research Fund of University of London. The authors are grateful for the countless advice and
471 information on manufacturing provided by Mr Anthony Otten and Mr Vince Ford.

472

473 7 References

- 474 [1] L. Kosnik, The potential for small scale hydropower development in the US, *Energy Policy* 38(10) (2010) 5512-5519.
- 475 [2] H. Siebert, *The Problem, Economics of the Environment*, Springer Berlin Heidelberg 2008, pp. 3-6.
- 476 [3] N. Stern, *The Economics of Climate Change*, The Stern Review, Cambridge University Press 2007.
- 477 [4] T. Korakianitis, S. Imran, D.R. Emberson, A.M. Namasivayam, R.J. Crookes, Internal Combustion Engine Performance and Emissions
- 478 Aspects When Fueled by Conventional and Sustainable Fuels, *Handbook of Clean Energy Systems*.
- 479 [5] M. Höök, X. Tang, Depletion of fossil fuels and anthropogenic climate change - A review, *Energy Policy* 52(0) (2013) 797-809.
- 480 [6] B. Ihracska, T. Korakianitis, P. Ruiz, D.R. Emberson, R.J. Crookes, A. Diez, D. Wen, Assessment of elliptic flame front propagation
- 481 characteristics of iso-octane, gasoline, M85 and E85 in an optical engine, *Combustion and Flame* 161(3) (2014) 696-710.
- 482 [7] B. Ihracska, D. Wen, S. Imran, D.R. Emberson, L. Maria Ruiz, R.J. Crookes, T. Korakianitis, Assessment of elliptic flame front propagation
- 483 characteristics of hydrogen in an optically accessible spark ignition engine, *International Journal of Hydrogen Energy* 38(35) (2013) 15452-
- 484 15468.
- 485 [8] S. Imran, D. Emberson, A. Diez, D. Wen, R. Crookes, T. Korakianitis, Natural gas fueled compression ignition engine performance and
- 486 emissions maps with diesel and RME pilot fuels, *Applied Energy* 124 (2014) 354-365.
- 487 [9] R.J. Crookes, Soot Formation and Oxidation at High Pressure in a Confined Spray Flame, *Combustion Science and Technology* 178(8)
- 488 (2006) 1491-1510.
- 489 [10] A. Demosthenous, Soot formation and oxidation in a high-pressure spray flame, Queen Mary, University of London, 2005.
- 490 [11] M.A.A. Nazha, R.J. Crookes, Design and Operation of a High-Pressure Combustion System for Study of Soot Formation, *SAE*
- 491 *International*, 1992.
- 492 [12] H. Zhao, N. Ladommatos, *Engine Combustion Instrumentation and Diagnostics*, SAE International 2001.
- 493 [13] H. Zhao, *Laser Diagnostics and Optical Measurement Techniques in Internal Combustion Engines*, 2012.
- 494 [14] D. Emberson, B. Ihracska, S. Imran, A. Diez, Optical characterization of Diesel and water emulsion fuel injection sprays using
- 495 shadowgraphy, *Fuel* 172 (2016) 253-262.
- 496 [15] J. Mackerle, Finite elements in the analysis of pressure vessels and piping, an addendum: A bibliography (2001–2004), *International*
- 497 *Journal of Pressure Vessels and Piping* 82(7) (2005) 571-592.
- 498 [16] H. Mayer, H. Stark, S. Ambrose, Review of fatigue design procedures for pressure vessels, *International journal of pressure vessels*
- 499 *and piping* 77(13) (2000) 775-781.
- 500 [17] R. Preiss, Design-by-analysis of a chemical reactor's head under sustained and thermal loads, *International journal of pressure vessels*
- 501 *and piping* 77(6) (2000) 277-288.
- 502 [18] M. Staat, M. Heitzer, H. Lang, K. Wirtz, Direct finite element route for design-by-analysis of pressure components, *International*
- 503 *Journal of Pressure Vessels and Piping* 82(1) (2005) 61-67.
- 504 [19] M.J. Hyder, M. Asif, Optimization of location and size of opening in a pressure vessel cylinder using ANSYS, *Engineering Failure Analysis*
- 505 15(1-2) (2008) 1-19.
- 506 [20] S. Chattopadhyay, *Pressure Vessels: Design and Practice*, CRC Press LLC 2005.
- 507 [21] J. Spence, D.H. Nash, Milestones in pressure vessel technology, *International Journal of Pressure Vessels and Piping* 81(2) (2004) 89-
- 508 118.
- 509 [22] D. Nash, M. Abid, Combined external load tests for standard and compact flanges, *International journal of pressure vessels and piping*
- 510 77(13) (2000) 799-806.
- 511 [23] H. Darijani, M.H. Kargarnovin, R. Naghdabadi, Design of thick-walled cylindrical vessels under internal pressure based on elasto-plastic
- 512 approach, *Materials & Design* 30(9) (2009) 3537-3544.
- 513 [24] S.M. Hosseini, Coupled thermoelasticity and second sound in finite length functionally graded thick hollow cylinders (without energy
- 514 dissipation), *Materials & Design* 30(6) (2009) 2011-2023.
- 515 [25] H.R. Zare, H. Darijani, A novel autofrettage method for strengthening and design of thick-walled cylinders, *Materials & Design* 105
- 516 (2016) 366-374.
- 517 [26] C. Nadarajah, L. Foo, Finite element study of keyed backing ring design for floating head, *International journal of pressure vessels and*
- 518 *piping* 75(6) (1998) 521-526.
- 519 [27] Schott, TIE-35: Transmittance of optical glass, 2005.
- 520 [28] Schott, TIE-31: Mechanical and Thermal Properties of Optical Glass, 2004.
- 521 [29] K.B. Doyle, M.A. Kahan, Design strength of optical glass, *Proceedings of SPIE* 5176 *Optomechanics* (2003) 14-25.
- 522 [30] Hoya, *Optical Glass: Specifications*.
- 523 [31] Schott, *Technical Glasses, Physical and technical properties*, 2010.
- 524 [32] ISO, *Optics and photonics -- Specification of raw optical glass*, 2010.
- 525 [33] M.J. Weber, *Handbook of Optical Materials*, CRC Press 2002.
- 526 [34] A.K. Koenig Spilman, *Stress-Engineered Optical Elements*, School of Engineering and Applied Sciences, University of Rochester, 2007.
- 527 [35] C.A. Klein, Characteristic strength, Weibull modulus, and failure probability of fused silica glass, *Optical Engineering* 48(11) (2009)
- 528 113401-113401-10.
- 529 [36] J. Detrio, D. Iden, F. Orazio, S. Goodrich, G. Shaughnessy, Experimental validation of the Weibull area-scaling principle, *Proc. 12th*
- 530 *DoD Electromagnetic Windows Symp*, 2008, p. 434.
- 531 [37] O.V. Voloshyn, L.A. Lytvynov, E.V. Slyunin, Potentialities for sapphire strength enhancement, *Functional Materials* 14(4) (2007) 569-
- 532 569.
- 533 [38] D.A. Ditmars, S. Ishihara, S.S. Chang, G. Bernstein, E.D. West, Enthalpy and Heat-Capacity Standard Reference Material: Synthetic
- 534 Sapphire Al₂O₃ From 10 to 2250 K, *JOURNAL OF RESEARCH of the National Bureau of Standards* 87(2) (1982) 159-159.
- 535 [39] L.S. Combes, S.S. Ballard, K.A. McCarthy, Mechanical and Thermal Properties of Certain Optical Crystalline Materials, *J. Opt. Soc. Am.*
- 536 41(4) (1951) 215-221.
- 537 [40] D.C. Harris, High-temperature strength of sapphire, *International Symposium on Optical Science and Technology*, International
- 538 *Society for Optics and Photonics*, 2000, pp. 25-36.
- 539 [41] F. Schmid, D.C. Harris, Effects of crystal orientation and temperature on the strength of sapphire, *Journal of the American Ceramic*
- 540 *Society* 81(4) (1998) 885-893.

541 [42] G. Wang, H. Zuo, H. Zhang, Q. Wu, M. Zhang, X. He, Z. Hu, L. Zhu, Preparation, quality characterization, service performance evaluation
542 and its modification of sapphire crystal for optical window and dome application, *Materials & Design* 31(2) (2010) 706-711.

543 [43] W. Wunderlich, H. Awaji, Molecular dynamics — simulations of the fracture toughness of sapphire, *Materials & Design* 22(1) (2001)
544 53-59.

545 [44] H.W. Icenogle, B.C. Platt, W.L. Wolfe, Refractive indexes and temperature coefficients of germanium and silicon, *Applied Optics* 15(10)
546 (1976) 2348-2351.

547 [45] A. Duncanson, R.W.H. Stevenson, Some Properties of Magnesium Fluoride crystallized from the Melt, *Proceedings of the Physical
548 Society* 72(6) (1958) 1001-1001.

549 [46] P. Laporte, J.L. Subtil, M. Courbon, M. Bon, L. Vincent, Vacuum-ultraviolet refractive index of LiF and MgF₂ in the temperature range
550 80–300 K, *Journal of the Optical Society of America* 73(8) (1983) 1062-1069.

551 [47] A. Diez, R.J. Crookes, T. Løvås, Experimental studies of autoignition and soot formation of diesel surrogate fuels, *Proceedings of the
552 Institution of Mechanical Engineers, Part D: Journal of Automobile Engineering* 227(5) (2013) 656-664.

553 [48] J.G. Williams, R.E. Anley, D.H. Nash, T.G.F. Gray, Analysis of externally loaded bolted joints: Analytical, computational and
554 experimental study, *International Journal of Pressure Vessels and Piping* 86(7) (2009) 420-427.

555 [49] A.-H. Bouzid, Comparative study of bolt spacing formulas used in bolted joint designs, *International Journal of Pressure Vessels and
556 Piping* 120-121 (2014) 47-54.

557 [50] T.J. Manuccia, J.R. Peele, C.E. Geosling, High temperature ultrahigh vacuum infrared window seal, *Review of Scientific Instruments*
558 52(12) (1981) 1857-1859.

559 [51] P.R. Yoder Jr, *Mounting Optics in Optical Instruments*, SPIE Press2008.

560 [52] P.R. Yoder Jr, *Opto-mechanical systems design*, SPIE Press2006.

561 [53] G. Dunn, J. Stachiw, Acrylic windows for underwater structures, *Underwater Photo Optics I*, International Society for Optics and
562 Photonics, 1966, pp. 157-168.

563 [54] G.M. Dunn, J.D. Stachiw, Acrylic Windows For Underwater Structures, *Proceedings of SPIE* 0007 (1966) 157-168.

564 [55] M. Abid, D.H. Nash, A parametric study of metal-to-metal contact flanges with optimised geometry for safe stress and no-leak
565 conditions, *International Journal of Pressure Vessels and Piping* 81(1) (2004) 67-74.

566 [56] BS EN, 13445-3: Unfired pressure vessels - Part3: Design, 2009.

567 [57] ASME, ASME Boiler and Pressure Vessel Code, Section VIII, Division 3, New York, 2004.

568 [58] A.T. Diamantoudis, T. Kermanidis, Design by analysis versus design by formula of high strength steel pressure vessels: a comparative
569 study, *International Journal of Pressure Vessels and Piping* 82(1) (2005) 43-50.

570 [59] D.C. Harris, *Materials for infrared windows and domes: properties and performance*, SPIE press1999.

571 [60] M. Specifications, *Optical Components for Fire Control Instruments; General Specification Governing the Manufacture, Assembly,
572 1963*.

573 [61] ISO, *Optics and photonics -- Preparation of drawings for optical elements and systems -- Part 8: Surface texture; roughness and
574 waviness*, 2010.

575 [62] R.J. Roark, *Formulas for Stress and Strain*, McGraw-Hill Book Co Inc., New York, 1954.

576 [63] W.C. Young, R.G. Budynas, *Roark's formulas for stress and strain*, McGraw-Hill New York2002.

577 [64] R.E. Fischer, B. Tadic-Galeb, P.R. Yoder, R. Galeb, *Optical system design*, McGraw Hill New York2000.

578 [65] D.R. Hearn, Vacuum window optical power induced by temperature gradients, *SPIE's International Symposium on Optical Science,
579 Engineering, and Instrumentation*, International Society for Optics and Photonics, 1999, pp. 297-308.

580 [66] R. Kingslake, R.B. Johnson, *Lens design fundamentals*, academic press2009.

581 [67] C.A. Klein, J. Pappis, ZnS, ZnSe, and ZnS/ZnSe windows: their impact on FLIR system performance, *Optical Engineering* 25(4) (1986)
582 254519-254519-.

583 [68] B. Ihracska, *Combustion of Alternative Fuels: Opto-Mechanical Design and Optical Investigation*, Queen Mary University of London,
584 2016.

585 [69] M.F. Ashby, *Materials selection in mechanical design*, Butterworth-Heinemann, Oxford, 2005.

586 [70] K.B. Doyle, M.A. Kahan, Design strength of optical glass, *Optical Science and Technology*, SPIE's 48th Annual Meeting, International
587 Society for Optics and Photonics, 2003, pp. 14-25.

588 [71] D. Vukobratovich, *Optomechanical Design Principles*, CRC Press LLC1999.

589 [72] J. Wannenburg, G.C. Klintworth, A.D. Raath, The use of probability theory in fracture mechanics—A case study, *International Journal
590 of Pressure Vessels and Piping* 50(1–3) (1992) 255-272.

591 [73] J. Daintith, *Oxford dictionary of physics*, Oxford University Press Oxford, 2005.

592 [74] M. Sparks, M. Cottis, Pressure-induced optical distortion in laser windows, *Journal of Applied Physics* 44(2) (1973) 787-794.

593 [75] R.K. Kimmel, R.E. Parks, *ISO 10110 Optics and Optical Instruments: Preparation of Drawings for Optical Elements and Systems: a
594 User's Guide*, Optical Society of America2002.

595 [76] D. Hasselman, Unified theory of thermal shock fracture initiation and crack propagation in brittle ceramics, *Journal of the American
596 Ceramic society* 52(11) (1969) 600-604.

597 [77] D. Li, W. Li, W. Zhang, D. Fang, Thermal shock resistance of ultra-high temperature ceramics including the effects of thermal
598 environment and external constraints, *Materials & Design* 37 (2012) 211-214.

599 [78] R. Delgado, M. Hallinan, 'Mounting of Lens Elements, *Opt. Eng* 14 (1975) 11.

600 [79] P.R. Yoder Jr, Parametric investigations of mounting-induced axial contact stresses in individual lens elements, *SPIE's 1993
601 International Symposium on Optics, Imaging, and Instrumentation*, International Society for Optics and Photonics, 1993, pp. 8-20.

602 [80] W. Chen, C. Nelson, Thermal stress in bonded joints, *IBM Journal of Research and Development* 23(2) (1979) 179-188.

603 [81] S. Timoshenko, J. Goodier, H.N. Abramson, Theory of elasticity, *Journal of Applied Mechanics* 37 (1970) 888.

604 [82] J.E. Greivenkamp, *Field Guide to Geometrical Optics*, Spie Press2004.

605 [83] W.P. Barnes Jr, Some effects of aerospace thermal environments on high-acuity optical systems, *Applied optics* 5(5) (1966) 701-711.

606 [84] M.C. Dudzik, *Electro-Optical Systems Design, Analysis, and Testing*, SPIE Optical Engineering Press1993.

607 [85] F. Shahabian, S.M. Hosseini, Stochastic dynamic analysis of a functionally graded thick hollow cylinder with uncertain material
608 properties subjected to shock loading, *Materials & Design* 31(2) (2010) 894-901.

- 609 [86] B. EN, 13445-3: 2009, BSI British Standards. Unfired pressure vessels-Part.
610 [87] A. Hafezalkotob, A. Hafezalkotob, Comprehensive MULTIMOORA method with target-based attributes and integrated significant
611 coefficients for materials selection in biomedical applications, *Materials & Design* 87 (2015) 949-959.
612 [88] S. Poulidikou, C. Schneider, A. Björklund, S. Kazemahvazi, P. Wennhage, D. Zenkert, A material selection approach to evaluate material
613 substitution for minimizing the life cycle environmental impact of vehicles, *Mater. Des* 83 (2015) 704-712.
614 [89] BS ISO, Fluid power systems. O-rings. Inside diameters, cross-sections, tolerances and designation codes, 2012.
615 [90] S.R. Lin, J.S. Yu, C.S. Chang, Stress analysis of screws in the fuel channel fastener assembly, *International Journal of Pressure Vessels
616 and Piping* 117-118 (2014) 49-55.
617 [91] BSI, PD 5500 Specification for unfired fusion welded pressure vessels, 2009.
618